Lab on a Chip

PAPER

Cite this: *Lab Chip*, 2017, **17**, 2125

Microfluidic-based high-throughput optical trapping of nanoparticles†

Abhay Kotnala, [a] Yi Zheng, [b] Jianping Fu [bcde] and Wei Cheng *[afg]

Received 17th March 2017,
Accepted 17th May 2017

DOI: 10.1039/c7lc00286f

rsc.li/loc

Optical tweezers have emerged as a powerful tool for multiparametric analysis of individual nanoparticles with single-molecule sensitivity. However, its inherent low-throughput characteristic remains a major obstacle to its applications within and beyond the laboratory. This limitation is further exacerbated when working with low concentration nanoparticle samples. Here, we present a microfluidic-based optical tweezers system that can 'actively' deliver nanoparticles to a designated microfluidic region for optical trapping and analysis. The active microfluidic delivery of nanoparticles results in significantly improved throughput and efficiency for optical trapping of nanoparticles. We observed a more than tenfold increase in optical trapping throughput for nanoparticles as compared to conventional systems at the same nanoparticle concentration. To demonstrate the utility of this microfluidic-based optical tweezers system, we further used back-focal plane interferometry coupled with a trapping laser for the precise quantitation of nanoparticle size without prior knowledge of the refractive index of nanoparticles. The development of this microfluidic-based active optical tweezers system thus opens the door to high-throughput multiparametric analysis of nanoparticles using precision optical traps in the future.

1. Introduction

Multiparametric characterization of nanoparticles at the single particle level is in tremendous demand for applications in nanomedicine,[1,2] photovoltaics,[3] clinical diagnosis,[4] environment,[5] and industry[6] among many others. Detection of individual nanoparticles with single-molecule sensitivity is important as they can directly reveal the heterogeneity among particles that is otherwise hidden in ensemble characterization. Single-molecule sensitivity is essential especially for biological particles, where a difference between particles of just one or two molecules could impart a measurable effect on their biological activity.[7] Furthermore, single-molecule sensitivity can offer an intrinsic reference based on which the stoichiometry of a particular protein in a biological nanoparticle can be estimated.[7,8] Such information is needed for better understanding and interpretation of experimental results. Many well-established microscopy techniques can be used for characterization of nanoparticles at the single-particle level. These include confocal laser scanning microscopy,[9] near-field scanning optical microscopy,[10] scanning electron microscopy,[11] transmission electron microscopy (TEM),[12] atomic force microscopy[13] and scanning tunneling microscopy.[14] New techniques such as nanoparticle tracking analysis,[15] nanopore integrated with resistive pulse techniques,[16] electronic detection[17,18] and optical detection[19,20] have also been used for characterization of size, concentration and other parameters of nanoparticles. Among these techniques, optical tweezers have emerged as a highly versatile tool for characterizing nanoparticles with unique advantages. First, optical tweezers allow detection of individual biological nanoparticles in fluid close to physiological conditions.[21] Second, optical tweezers allow detection of nanoparticles on the basis of an optical gradient force acting on the nanoparticle, which has a cubic dependence on the size of particles as compared to the sixth power dependence of scattering, thus providing higher sensitivity for size characterization compared to scattering based techniques.[22] Third, optical tweezers allow quantitation of nanoparticle size without prior knowledge of the refractive index of particles, which is a parameter necessary for size analysis based on light scattering techniques. For example, recently, optical

[a] *Department of Pharmaceutical Sciences, University of Michigan, 428 church street, Ann Arbor, MI 48109, USA*
[b] *Department of Mechanical Engineering, University of Michigan, 2350 Hayward street, Ann Arbor, MI 48109, USA*
[c] *Department of Biomedical Engineering, University of Michigan, Ann Arbor, Michigan 48109, USA*
[d] *Department of Cell and Developmental Biology, University of Michigan Medical School, Ann Arbor, MI 48109, USA*
[e] *Michigan Center for Integrative Research in Critical Care, University of Michigan, Ann Arbor, MI 48109, USA*
[f] *Department of Biological Chemistry, University of Michigan Medical School, Ann Arbor, MI 48109, USA. E-mail: chengwe@med.umich.edu*
[g] *Department of Biophysics, University of Michigan, Ann Arbor, MI 48109, USA*
† Electronic supplementary information (ESI) available. See DOI: 10.1039/c7lc00286f

tweezers were used to determine the size and refractive index of individual HIV virions.[21,23] Fourth, optical tweezers can be integrated easily with other techniques such as fluorescence microscopy,[24] Raman spectroscopy,[25,26] atomic force microscopy (AFM)[27] and electrical characterization techniques,[28] which makes this technique rather versatile for multiparametric analysis of nanoparticles on a single platform. For example, optical tweezers coupled with two-photon fluorescence excitation have been used to determine the envelope protein density of HIV viruses[7,21] and for quantitative detection of carcinoembryonic antigen,[29] a cancer marker in human whole serum. Optical tweezers have also been used in combination with an external electric field to measure the charge carried by individual microparticles and optical anisotropy.[30] Another category of optical tweezers popularly known as nanophotonic tweezers has also shown nanoparticle characterization capabilities. For example, open microcavities were used for calculating the nanoparticle polarizability and coefficient of friction.[31] Lastly, the ability to manipulate individually trapped nanoparticles may permit sorting of individual particles based on measurement characteristics, an important but underexplored area. In spite of these unique features of optical tweezers, their low throughput characteristic[32,33] presents a major challenge in its development as a multiparametric characterization tool for nanoparticles. A high-throughput capability is practically necessary to improve the efficiency of data collection when working with samples containing a low concentration of nanoparticles such as HIV virions in human blood[34] or trying to detect rare particles such as titanium oxide (TiO_2) in the tertiary effluent of wastewater plants.[35]

Two major approaches, namely, time sharing of a laser beam[36] and holography,[37] have been developed for improving the throughput of optical tweezers. Both approaches are based on the idea of transforming optical trapping into a parallel process by creating multiple trapping points to enable simultaneous capture of multiple particles, thereby effectively increasing the throughput of optical tweezers. Although these techniques can increase the throughput of optical trapping, their applications in trapping and detection of sub-micron particles may still be limited. For example, for holographic tweezers, the input laser power is shared among all trapping points, and therefore it would require a high laser power for creating multiple traps to stably capture sub-micron particles. Using a relatively low laser power, plasmonic tweezers made of circular gold disks[38] and photonic waveguides[39] have been used to create multiple traps. However, simultaneous detection of multiple trapped particles is usually through imaging using a charged coupled device (CCD) camera, which is only suitable for sub-micron particles under special illumination conditions.[40,41]

In this work, we maintain optical trapping as a serial process, *i.e.*, trapping and analysing particles one at a time, but aim to increase the throughput of the system by speeding up the trapping process. This idea is based on the simple fact that an intrinsic bottleneck that limits the throughput of optical trapping is the time required for diffusing nanoparticles to encounter the diffraction-limited laser trap, which increases substantially for low concentration samples. We refer to such optical tweezers system, where particles encounter the laser trap only through normal diffusion without external influences of flow, electric or magnetic field *etc.*, as passive trapping systems. To ameliorate this bottleneck, here we integrate optical tweezers with a tapered microfluidic nanoparticle delivery system, where the microfluidic flow actively delivers target nanoparticles to the laser trap region. Thus, we term this design as an active trapping system. Specifically, the trapping laser was positioned in the smallest cross-section of the microfluidic channel to increase the probability of target nanoparticles encountering the trap region and therefore maximize the nanoparticle trapping efficiency. We found that the throughput of the microfluidic-based active trapping system is dependent on both the flow rate and the particle trapping efficiency. Both the throughput and trapping efficiency can be significantly improved by optimizing the flow rate. Moreover, the use of flow and a small cross-section channel to realize high throughput trapping does not impact the capability of the optical trap to characterize different features of nanoparticles, such as particle size. Applications of the microfluidic-based active trapping system can be extended for multiparametric measurements of nanoparticles while maintaining its high throughput feature. Other approaches can be combined with the presented technique with some modifications in the future to further increase the throughput of the optical tweezers system.

2. Material and methods

Microfluidic channel design

The schematic of the microfluidic channel used for trapping of nanoparticles is shown in Fig. 1a. The channel consists of three sections: input section, middle section and output section. The trapping laser propagates along the Z direction. The input and output sections are of width (w) 200 μm along the Y direction. The middle section consists of a symmetrical tapered structure with varying channel widths. The widths of the channel are 80, 40, 20 and 10 μm in the middle section, as shown in Fig. 1a. The height (h) of the channel along the Z direction is kept constant at 10 μm, as shown in Fig. 1d. Fig. 1b shows a microscopy image of the fabricated polydimethylsiloxane (PDMS) microfluidic channel taken using a 10× objective lens. The minimum cross-sectional size of the channel in the middle section is thus 10 μm × 10 μm (width (w) × height (h)), which is sufficiently small compared to our previous design (3000 μm × 100 μm in width (w) × height (h)) to potentially 'focus' nanoparticles to the trapping region and yet large enough to reduce the interference of the laser beam from the channel boundaries. The width of the input and output sections was fixed to 200 μm because a larger width easily led to channel collapse during fabrication as a result of the large aspect ratio (width to height ratio). PDMS-based channels with an aspect ratio of greater than 20 : 1

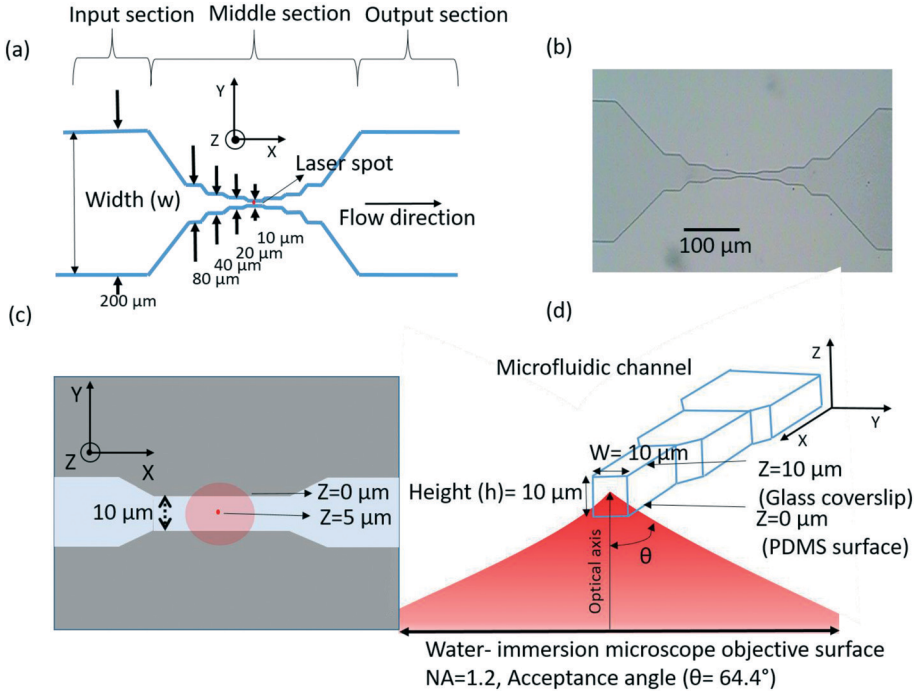

Fig. 1 (a) Schematic of the microfluidic channel used for the flow of nanoparticles. (b) Microscopy image of the fabricated PDMS-based channel using a 10× objective lens. (c) Schematic of the top view of a 10 μm section of the microfluidic channel showing the laser spots at two axial planes along the *Z* (height) direction. (d) Cross-sectional view of the 10 μm section of the channel showing the trap laser beam position with respect to the channel boundaries in the *Y* and *Z* directions.

tend to collapse during fabrication and therefore require additional supporting mechanisms which increases the complexity in the fabrication process.[42] Smaller channel widths for the input and output sections are also not recommended in our case. This is due to the long length (25.4 mm) of the input and output sections of the channel, which results in a high fluidic resistance and therefore would require high input pressure for the fluid flow. Such high pressure might damage the PDMS–glass bonding. The use of other materials like glass for the microfluidic channel fabrication could reduce some of these restrictions, but again they have a complex fabrication procedure as compared to the well-established fabrication procedure for PDMS-based microfluidic devices. A total of seven identical channels were fabricated on a single microfluidic device. This gives the microfluidic chip the flexibility of using different nanoparticle suspensions on the same device and also provides redundancy in the event of a channel failure due to clogging or other issues.

Chip fabrication

The microfluidic chamber was prepared using the standard soft lithography technique,[43] as shown in Fig. 2. The spacing between the objective and the condenser lenses in the experimental set-up ($f_{\text{objective}} + f_{\text{condenser}} = 540$ μm) requires the total microfluidic device thickness to be within ~440 μm

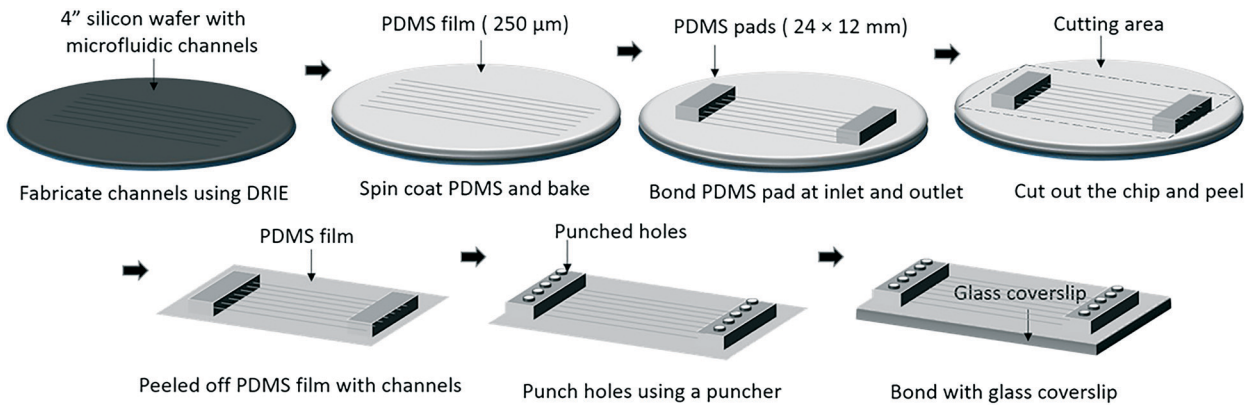

Fig. 2 Fabrication procedure of the microfluidic device using soft lithography.

(leaving 50 μm + 50 μm for DI water as a water-immersion objective lens is used for optical trapping, see the ESI† Fig. S1 for illustration). Since a no. 1 glass coverslip (130–170 μm) was used for bonding with the PDMS, the PDMS film containing the channels was fabricated to have a thickness of approximately 250 μm. The fabrication of such thin PDMS film requires a minor modification in the standard fabrication procedure used for microfluidic devices. The mould used for fabricating the microfluidic channels was made on a silicon wafer using deep reactive ion etching. This method allows the channels to have straight walls, in addition to a robust structure. A 10 : 1 mixture of PDMS base and curing agent was spin coated onto the silicon wafer containing the channels at a speed of 300 rpm for 45 seconds. This resulted in a thickness of around 250 μm for the PDMS film. The PDMS was then baked at 100 °C for 30 min. Due to the thin PDMS film, it is not possible to punch holes and apply tubing connectors to the PDMS film, which is to be bonded to the glass coverslip. To overcome this problem, we used two PDMS pads of size 24 × 12 mm and bonded them near the inlet and the outlet of the channels using oxygen plasma. Though this increases the thickness of the microfluidic device at the inlet and outlet of the channel, it maintains the thickness of 250 μm near the centre of the channels. This additional step was carried out prior to the peeling off of the PDMS film from the silicon wafer. The whole assembly of the PDMS film and the PDMS pads was then peeled off from the silicon wafer and now holes could be easily punched at the input and output ports for connecting the tubing. Finally, the PDMS film was bonded to the glass coverslip using oxygen plasma and baked at 60 °C for 15–30 min.

Optical tweezers experiment

A home-made optical tweezing instrument using a tapered amplifier diode laser operating at an air wavelength of 830 nm (SYS-420-830-1000, Sacher LaserTechnik LLC) was used for optical trapping of polystyrene nanoparticles.[44] In brief, the trapping laser was focused to a diffraction-limited spot using a 60× water-immersion objective lens with a numerical aperture of 1.2. The back-focal-plane interferometry (BFPI)[45] signal from the trapped particles was detected using a position sensitive detector (PSD) and recorded at 62.5 KHz for 10 seconds for the calculation of the diameter of nanoparticles.[46] The trap laser power was monitored using the PSD and kept constant at 130.8 mW with 1% variation at the focus for all the experiments. In the case of experiments using fluorescent polystyrene particles, a solid-state laser with a wavelength of 488 nm was used for their excitation and the epi-fluorescence was detected using an electron-multiplying charge-coupled device (EMCCD) camera. To measure the diameter of nanoparticles using a reference signal, a closed loop nano-positioning stage (3D200, Mad City Labs) was used to oscillate the microfluidic chamber along the *X* axis at a defined frequency and amplitude.[47] We notice that channel boundaries had no influence on the BFPI signal when the chamber was oscillated along the *X* axis, as compared to the oscillation along the *Y* axis, which would introduce unwanted noise to the BFPI signal due to the periodic change in the refractive index experienced by the laser beam due to moving channel boundaries. Thus, all particle sizing was done by oscillation of the chamber along the *X* axis. All the trapping experiments were conducted at a constant temperature of 20.0 ± 2 °C. The polystyrene nanoparticles were diluted in Milli-Q water to specified concentrations and sonicated before injection into the microfluidic channel. A pressure driven flow system was used for the flow of the nanoparticles in the microfluidic channel. We recommend the use of a pressure driven flow as compared to the mechanical flow using a syringe pump as the latter showed a very large relaxation time and lacked precise control of the flow rate during the experiments. The precise control of the flow rate is crucial for high throughput optical trapping as will be explained in a later section.

Measurement of trapping throughput

In this work, we quantify the throughput of optical trapping using the trapping frequency, which is the number of particles trapped per second. The experiments were conducted using polystyrene nanoparticles of two different sizes: one with an average diameter of 190 nm which is non-fluorescent and has been used extensively in the past for various calibration purposes,[21] and the other with an average diameter of 410 nm which is fluorescent and can be visualized using epi-fluorescence for measurement of trapping efficiency. The working concentrations for the 190 nm particles were kept constant at 4×10^7 particles per ml in all experiments. This concentration was calculated based on manufacturer-specified stock concentrations of the particle. The working concentrations for the 410 nm particles were kept constant at 2×10^7 particles per ml in all experiments. This range of concentrations was chosen to be close to the concentration of nanoparticles that we have studied previously, which represents a physiologically relevant concentration for virus particles. The concentration of the 410 nm fluorescent polystyrene particles was verified by direct counting of the particles under the microscope as described in the ESI.† In the active trapping system, the flow was maintained to deliver the particles and the flow velocity never exceeded the escape velocity of the trapped particles, which corresponds to the maximum flow velocity beyond which the particles cannot be trapped by the laser beam for a given laser power. The escape velocity of the trap in our experiment was found to be 1820 ± 50 μm s^{-1} for the 410 nm and 258 ± 10 μm s^{-1} for the 190 nm nanoparticles at the specified laser power. In contrast, in the passive trapping system, no flow was applied while the particles were trapped. For both systems, multiple particles were consecutively trapped and then released immediately in less than a second and the time stamp of each trapping event was recorded, either from the captured video in the case of the fluorescent nanoparticles or from the time series of the BFPI

signal, where a change in the BFPI signal indicates trapping of a particle.[23] The time interval between two consecutive trapping events gives the inter-particle trapping time and its inverse yields the trapping frequency. Throughout, the flow velocity in each section of the channel was measured from the flow videos of the 410 nm fluorescent particles passing through each section in the channel.

3. Results and discussion

High throughput optical trapping

We measured the trapping frequency in the active delivery trapping system and compared it with that in a passive trapping system, as described in Material and methods. Fig. 3a and b show a side-by-side comparison of the trapping frequencies for both the active and passive trapping systems, for both 190 nm and 410 nm polystyrene particles, respectively. The trapping frequency reported for the active trapping system was measured in the channel section with the smallest width (10 μm). At a flow rate of 190 ± 10 μm s^{-1}, the trapping frequency for the 190 nm particle was 0.04 ± 0.007 particles per second, which was slightly more than tenfold higher than that in the passive trapping system. The frequency of trapping varies with the flow rate (for more details see the dedicated section below). Throughout, the errors we reported for the flow velocity and trapping frequency are the standard error of the mean or SEM, unless otherwise noted. Similarly, the trapping frequency for the 410 nm particle was 0.4 ± 0.02 particles per second at a chosen flow rate of 1411 ± 35 μm s^{-1}, which was 30× higher than that in the passive trapping system. These results show that the throughput for optical trapping of nanoparticles can be improved substantially by using the tapered microfluidic nanoparticle delivery system. Two major factors likely contribute to the higher throughput: (1) the increase in the probability of particle trapping, due to the use of a microfluidic channel with small cross-sections and (2) the use of fluid flow for the delivery of nanoparticles rather than relying on normal diffusion. To quantify the influence of these two factors on the throughput of optical trapping, we have thus studied the trapping frequency as a function of the size of the channel cross-sections and the flow rate.

Impact of channel width on the trapping throughput at a set pressure

The channel section with the smallest width of 10 μm was used in the above experiments to measure the throughput of optical trapping, as its small size likely increases the chance to trap particles flowing across the channel. To further test this, we positioned the trapping laser in different sections of the microchannel and measured the trapping frequency in channel sections of different widths. In these experiments, a single setting of pneumatic pressure was applied to drive the flow in the microchannel. Although the linear flow velocity in each section varies with the width of the channel (Table 1), the input pressure was low enough such that the maximum flow velocity obtained in the channel (the highest in the 10 μm channel for a given input pressure) remained less than the escape velocity of the particles. Fig. 4a and b show the trapping frequency as a function of the channel width for both 190 nm and 410 nm particles. The results show clearly that the trapping frequency decreases considerably as the width of the channel is increased. This trend is true for both 190 and 410 nm particles. As a result, the channel section with the smallest width (or smallest cross-section) has the highest trapping frequency among all and therefore provides the highest throughput observed. For both 190 and 410 nm particles, the trapping frequencies became comparable to those in the passive trapping system when the channel section with the largest width of 200 μm was used for trapping. These results are consistent with the idea that a smaller cross-section can effectively 'focus' nanoparticles to the trapping region, which increases the probability of particles encountering the optical trap and thereby the throughput of optical trapping. However, it is worth noting that a higher flow rate

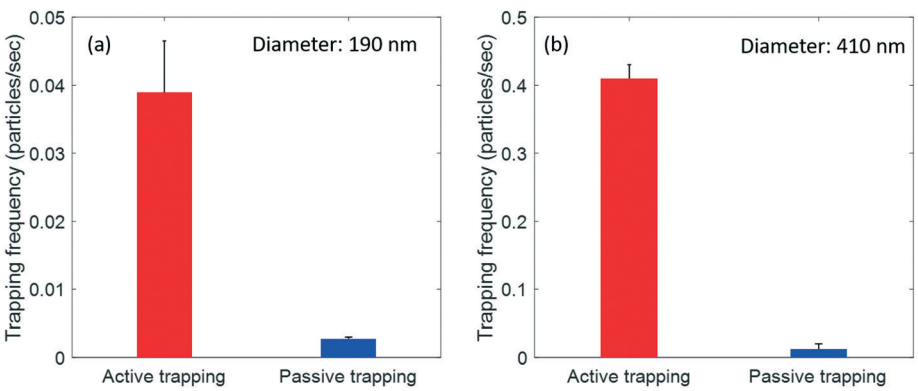

Fig. 3 Comparison of the trapping frequencies between the active and passive trapping systems (a) for the 190 nm polystyrene nanoparticles and (b) for the 410 nm fluorescent polystyrene nanoparticles. The error bar represents the SEM with sample sizes of N = 60 (active trapping) and N = 46 (passive trapping) for 190 nm polystyrene nanoparticles and N = 127 (active trapping) and N = 200 (passive trapping) for 410 nm polystyrene nanoparticles. The measured flow velocity in the case of active trapping is 190 ± 10 μm s^{-1} for the 190 nm polystyrene nanoparticles and 1411 ± 35 μm s^{-1} for the 410 nm polystyrene nanoparticles.

Table 1 Linear flow velocity as measured from the travel speed of particles in different sections of the channel during the trapping frequency measurements using the 190 and 410 nm polystyrene particles

Width (μm)	Flow velocity for 190 nm particles (μm s^{-1})	Flow velocity for 410 nm particles (μm s^{-1})
10	190 ± 10	485 ± 33
20	75 ± 5	240 ± 13
40	32 ± 2	109 ± 6
80	16 ± 1	54 ± 2
200	6 ± 0.5	26 ± 1

in thinner channels may also contribute to the increase in trapping frequency (see the "Impact of flow velocity on particle trapping efficiency and throughput" section). From these results, one can also predict that the throughput of optical trapping at a set pressure can be further improved by decreasing the cross-section of the channel, provided that the small channel can be fabricated and nonspecific interactions are minimal between the particles and the channel walls.

Impact of channel width on the particle trapping efficiency at a set pressure

A corollary of the above results is that the efficiency of trapping particles would be increased with decreasing channel cross-sections. The rationale is that decreasing the channel cross-sections will effectively increase the fraction of fluid volumes that carry particles crossing the trapping region of the laser beam, such that a larger fraction of particles will be under the influence of the optical trap, which increases the probability of trapping. In this section, we demonstrate this effect by measuring the trapping efficiency, which is a direct measure of this increase in the probability of trapping leading to higher throughput of the optical trapping system. Trapping efficiency is defined as the percentage of particles trapped *versus* the total number of particles passing through the channel.

$$\text{Trapping efficiency} = \frac{n_{\text{trap}}}{n_{\text{flow}}} \times 100$$

n_{flow}: total number of particles flowed

n_{trap}: number of particles trapped

To obtain a reliable measure of the total number of particles traversing through the microfluidic channel, we used epi-fluorescence to directly visualize and count the 410 nm fluorescent particles. The particle trapping efficiency was then measured by trapping fluorescent polystyrene particles in different sections of the microfluidic channel. The total number of particles trapped and flowed across the channel was counted from the flow video of the fluorescent particles in the channel captured by an EMCCD. Fig. 5 shows the particle trapping efficiency in the 10, 20, 40, 80 and 200 μm sections of the microfluidic channel obtained from the 410 nm fluorescent particles. From the results, we observe a significant decrease in particle trapping efficiency from 33% to 3.1% when the width of the channel is increased from 10 μm to 200 μm. The result clearly demonstrates that the small cross-section of the channel results in an increased probability of trapping of particles flowing across it and hence a higher particle trapping efficiency. Though the direct measurement of the particle trapping efficiency for the 190 nm nanoparticles was not possible, as being non-fluorescent, we cannot count the total number of particles flowed across the channel, but based on the channel dimension, flow velocity measurement (obtained by mixing the 410 nm fluorescent particles in the 190 nm nanoparticle solution) and the given concentration of the 190 nm nanoparticles, we could estimate the total number of particles flowed across the channel section in a given time frame. Thus, based on the number of particles trapped and the estimated number of particles flowed across the channel in a particular time frame, we found a particle trapping

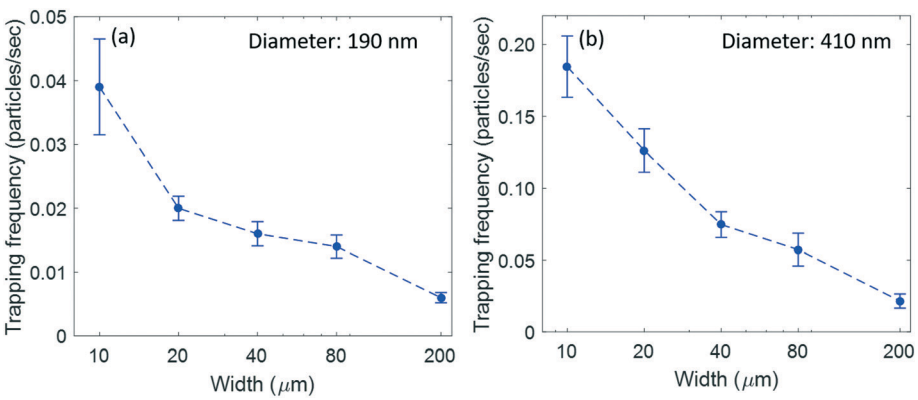

Fig. 4 Trapping frequency as a function of the width of the channel used for the optical trapping of (a) 190 nm polystyrene particles and (b) 410 nm polystyrene particles. The error bars represent the SEM with sample sizes of N = 60 (W = 10 μm), N = 41 (W = 20 μm), N = 33 (W = 40 μm), N = 30 (W = 80 μm), and N = 27 (W = 200 μm) for 190 nm polystyrene nanoparticles and N = 36 (W = 10 μm), N = 49 (W = 20 μm), N = 34 (W = 40 μm), N = 41 (W = 80 μm), and N = 13 (W = 200 μm) for 410 nm polystyrene nanoparticles.

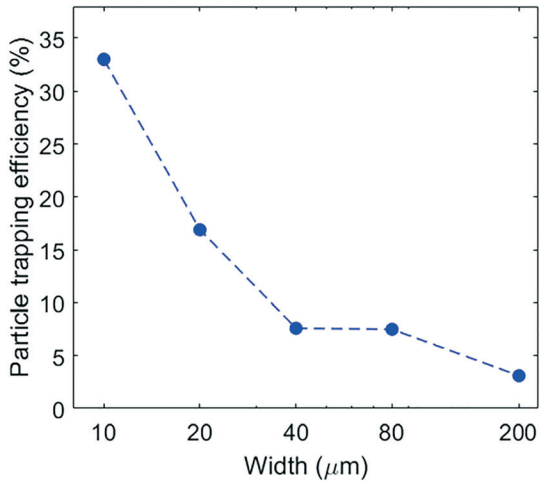

Fig. 5 Particle trapping efficiency variation with change in the width of the microfluidic channel. The flow velocity for each section is given in Table 1.

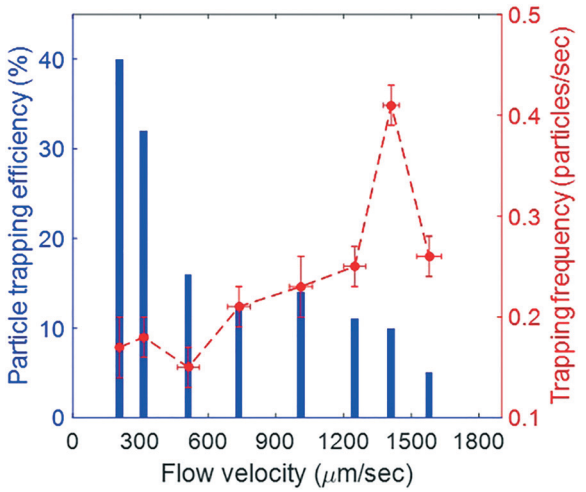

Fig. 6 Particle trapping efficiency (blue, left) and trapping frequency (red, right) in the 10 μm width channel section at different flow velocities. The error bars in X and Y represent the SEM with sample sizes of N = 68 (v = 208 ± 14 μm s^{-1}), N = 84 (v = 315 ± 17 μm s^{-1}), N = 61 (v = 512 ± 48 μm s^{-1}), N = 69 (v = 736 ± 50 μm s^{-1}), N = 56 (v = 1249 ± 49 μm s^{-1}), N = 127 (v = 1411 ± 35 μm s^{-1}), and N = 69 (v = 1580 ± 54 μm s^{-1}) for trapping frequency measurement and N = 10 for flow velocity measurement.

efficiency of 2.8% at a flow velocity of 190 ± 10 μm s^{-1} and 4.3% at 147 ± 11 μm s^{-1} in the 10 μm section.

Impact of flow velocity on particle trapping efficiency and throughput

The application of flow, in principle, can 'speed up' the delivery of particles to the trap region and thus increase the throughput of the system. On the other hand, a flow velocity above a certain threshold may generate a Stokes force that is large enough to simply compete with the trapping potential and thus decrease both the throughput and efficiency of trapping. Given the importance of flow velocity in this active trapping system, it is necessary to study its impact on the particle trapping frequency and efficiency. To this end, we used a pneumatic pressure system to drive fluid at different velocities in the channel. The trapping frequency and efficiency were both measured in the 10 μm section at different flow velocities using the 410 nm fluorescent polystyrene particles. As shown in Fig. 6, the particle trapping efficiency was reduced from 40% at 208 μm s^{-1} to 5% for a flow velocity of 1580 μm s^{-1}. All these flow velocities were lower than the escape velocity of the particles, and yet the trapping efficiency decreases with the increase in the flow velocity. This is because at high flow velocity, only particles that encounter the centre of the trap's potential well (the focus of the laser beam) are trapped, whereas the particles that travel slightly away from the centre of the potential well escape the trap. The reason for this is that a high flow velocity yields a very short lifetime of the particles under the influence of the trap potential. In contrast, with lower velocities at which the particles flow across the trap region, they spend a longer time in the trap region, which increases the probability of the particle being pulled into the trap. Thus, more particles passing through the trap region are trapped. This explains the decrease in the particle trapping efficiency with the increase in flow velocity. However, the trapping frequency does not follow the same behaviour as the particle trapping efficiency (Fig. 6), which displays a pronounced peak dependence on the flow velocity. The increase in flow velocity increases the rate of delivery of nanoparticles to the trapping region for a given concentration of particles and thereby is meant to increase the throughput; however, this increase is counteracted by the decrease in particle trapping efficiency with the increase in flow velocity as described earlier. This result is important and shows that an optimal flow velocity exists in order to maximize the trapping throughput. This optimal flow velocity would not exceed the escape velocity of the particle, which corresponds to the maximum flow velocity beyond which the particle will be no longer trapped for a given laser power (see Material and methods for measured escape velocities).[48]

Application of high throughput optical tweezers for determination of nanoparticle size

In our earlier works, passive trapping of nanoparticles using a regular microfluidic chamber has been used to determine parameters such as size (diameter) and refractive index (n) of polystyrene nanoparticles and HIV virions.[21,23] In this section, we show that our high throughput optical tweezers system can still perform nanoparticle characterization, even though it operates in a flow-based environment and uses a microfluidic channel with a small cross-section, in contrast to the passive trapping system. We demonstrate this by using the present trapping system to determine the diameter of the nanoparticles, but it can be extended to study other

parameters also, as was done previously using the passive trapping system. Polystyrene particles with an average diameter of 190 nm and 410 nm, respectively, were optically trapped using the 'active' trapping system. The power spectrum calibrated using chamber oscillation was then used to determine the size of the nanoparticles as described previously.[21] Fig. 7a shows a representative BFPI signal of a trapped 190 nm polystyrene nanoparticle in this microfluidic channel. Fig. 7b shows the power spectrum obtained from the BFPI data and was calculated as described.[21] The power spectrum of the Brownian motion of the nanoparticles in an optical trap is best interpreted using the Einstein–Ornstein–Uhlenbeck theory of Brownian motion, which predicts a Lorentzian spectrum.[49] Hence, the power spectrum was fitted to a Lorentzian following the procedure as we described previously,[21] which gives the diffusion constant (D_v) in volts^2 per second and the corner frequency (f_c) in Hz. Oscillation of the chamber was used to determine the calibration factor (β) to convert D_v from units of volts^2 per second to $\mu m^2\ s^{-1}$. The values obtained from the Lorentzian fit and the chamber oscillation were then used to determine the size of the trapped particle. Fig. 8a and b show the histograms of the diameter values obtained from the power spectrum analysis of the BFPI signal of the trapped 190 nm (N = 108) and 410 nm (N = 52) polystyrene particles. The diameters obtained are 200 ± 48 nm and 409 ± 64 nm (mean ± standard deviation), respectively, which agree well with the diameter values of 184 ± 12 and 403 ± 6 (mean ± standard deviation) measured using TEM as shown in ref. 21 and in the Fig. 8b inset respectively for the 190 nm and 410 nm particles. The active trapping system can thus accurately determine the size of trapped nanoparticles and has the capability to do multiparametric analysis of nanoparticles with high throughput.

Impact of fluid flow velocity on the power spectrum analysis

The trapping of the nanoparticles and the collection of the BFPI signal obtained from the trapped particle was carried out in a fluid flow environment as opposed to the no-flow based passive trapping system. This makes it necessary to study the impact of fluid flow on the BFPI signal and the corresponding power spectrum of the trapped particle. Any deviation in the power spectrum with the change in the fluid flow velocity would influence the accurate calculation of the size of the trapped particle. The influence of fluid flow was studied experimentally by trapping a single 410 nm polystyrene nanoparticle and subsequently recording the BFPI signal while incrementing the fluid flow velocity from a low value of 10 $\mu m\ s^{-1}$ to 345 $\mu m\ s^{-1}$ (less than the escape velocity of the trap). Fig. 9a shows the BFPI signals obtained from the trapped particle at different flow velocities. We did not observe any significant change in the BFPI signal, except a small change in the mean level of the BFPI signal. The change in the mean level of the BFPI signal with the increase in the fluid velocity corresponds to an increase in the displacement of the particle from the centre of the trap. The increase in the flow velocity increases the drag force proportional to the fluid velocity, which changes the equilibrium position of the trapped particle, resulting in the change in the mean level of the BFPI signal. The power spectra obtained from the corresponding BFPI signal at different fluid velocities are plotted in Fig. 9b. We find again that the change in the flow velocity resulted in a little change in the power spectrum as the fluid velocity was increased. The diffusion coefficient D_v and the corner frequency f_c obtained from the fitting of the power spectrum showed only a 6.3% and 4.1% variation even though the change in the fluid velocity was more than 30-fold. The diameter of the trapped particle

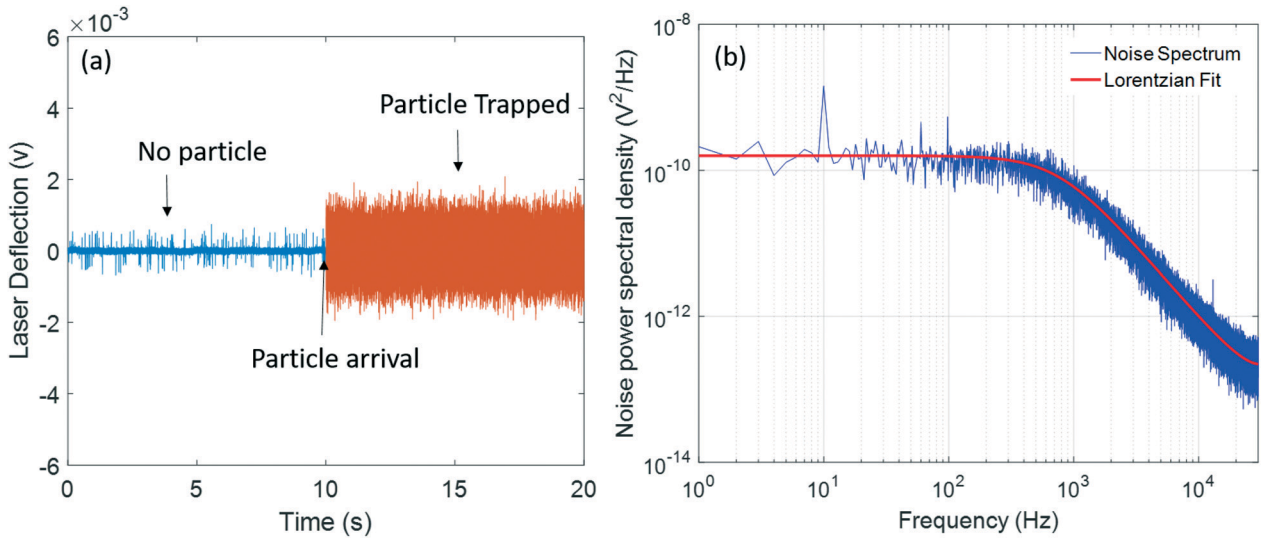

Fig. 7 (a) Representative BFPI signal with no particle and with a 190 nm polystyrene particle in the optical trap. (b) Power spectrum of the BFPI data obtained from the trapped particle from (a) with a Lorentzian fit.

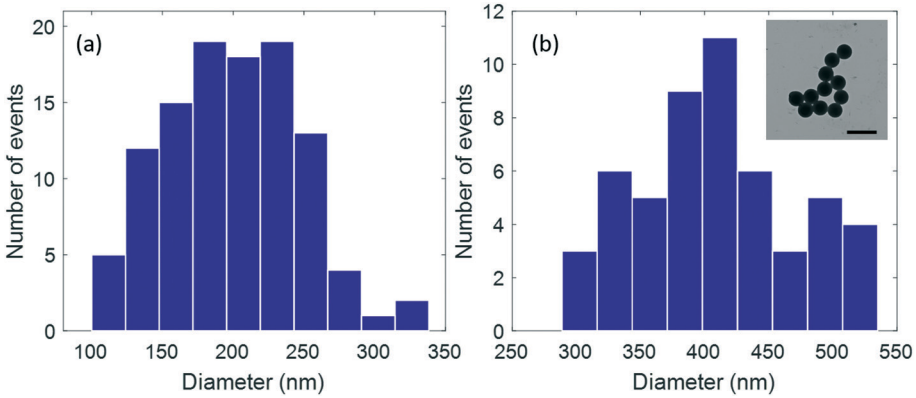

Fig. 8 Diameter values of trapped polystyrene nanoparticles calculated using the power spectrum analysis of the BFPI data obtained from trapping of (a) 190 nm polystyrene particles and (b) 410 nm polystyrene particles. (Inset) TEM image of 410 nm polystyrene particles, scale bar: 800 nm.

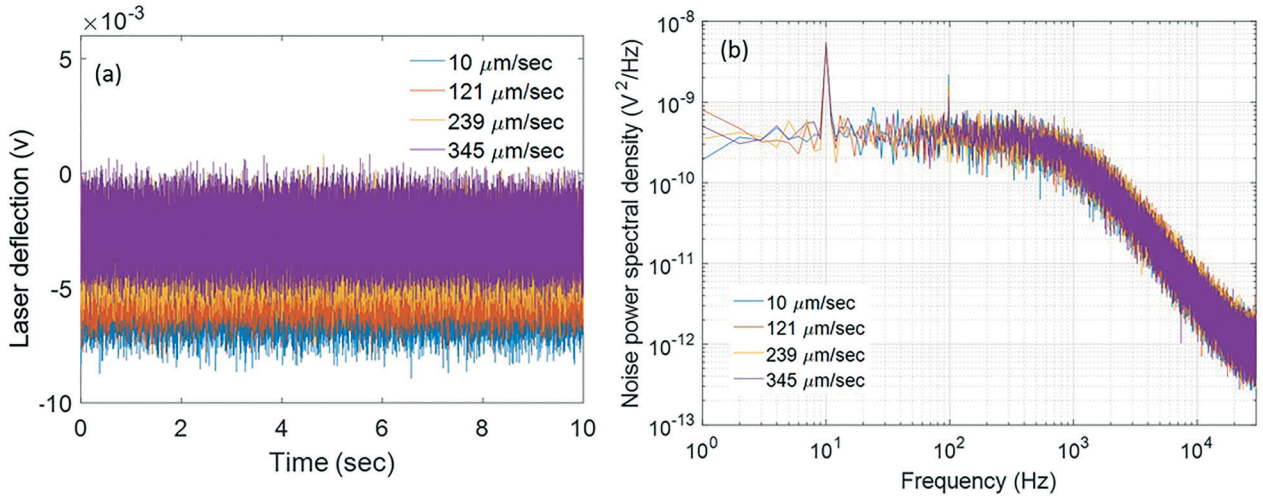

Fig. 9 (a) BFPI signal obtained from the trapped 410 nm polystyrene particle at different flow velocities. (b) Power spectra of the BFPI data obtained from (a) at different flow velocities.

that we derived from the power spectrum analysis showed a coefficient of variation of only 6%, which shows no significant influence of flow velocity on the measurement of particle size. The flow only adds a constant force, called the drag force $F = 6\pi\eta r v$ with no time dependence and hence makes no contribution to the power spectrum. The power spectrum is a result of random Brownian motion of the particle in the trap due to thermal forces, and hence independent of the flow. The results, as shown in Fig. 9, suggest the harmonic nature of the optical trap.[44] When the flow velocity approaches the escape velocity of the trapped particle, the BFPI signal may show deviations from the expected behavior. How to extract particle size information from these unstable trapping conditions will be a subject of future research.

Conclusions

As optical tweezers continue to grow as a multiparametric characterization tool for nanoparticles, there is a strong need to address their low throughput characteristic. In this paper, we have shown that an optical trapping system, based on the active delivery of nanoparticles, results in a significant increase in the throughput of optical tweezers. The throughput is increased more than ten-fold as compared to a passive trapping system. The impact of two important parameters of this trapping system, the flow velocity and microfluidic channel dimensions, on the throughput were also studied, showing that the use of the smallest cross-section channel for trapping along with an optimized flow velocity results in the maximum trapping throughput. Despite the application of flow in a spatially-confined channel cross-section, the active tweezers system maintains the same functionality as the passive trapping system. We demonstrated this by using the trapping system to measure the size of polystyrene nanoparticles. The mean size obtained was found to match very well with the measured diameter values using TEM. This technique has the potential to develop into a versatile multiparametric tool for the characterization of biological nanoparticles.

Acknowledgements

This work was supported by the National Science Foundation (CAREER Award CHE1149670, WC; CMMI 1536087, JF) and the National Institutes of Health (Director's New Innovator Award 1DP2OD008693-01, WC). Dr. Y. Zheng is partially supported by the Natural Sciences and Engineering Research Council of Canada (NSERC) Postdoctoral Fellowship.

References

1 K. N. Sugahara, T. Teesalu, P. P. Karmali, V. R. Kotamraju, L. Agemy, O. M. Girard, D. Hanahan, R. F. Mattrey and E. Ruoslahti, *Cancer Cell*, 2009, **16**, 510–520.
2 W. H. De Jong and P. J. A. Borm, *Int. J. Nanomed.*, 2008, **3**, 133–149.
3 M. A. Franzman, C. W. Schlenker, M. E. Thompson and R. L. Brutchey, *J. Am. Chem. Soc.*, 2010, **132**, 4060–4061.
4 M. Verma, T. K. Lam, E. Hebert and R. L. Divi, *BMC Clin. Pathol.*, 2015, **15**, 6.
5 W. T. Liu, *J. Biosci. Bioeng.*, 2006, **102**, 1–7.
6 W. J. Stark, P. R. Stoessel, W. Wohlleben and A. Hafner, *Chem. Soc. Rev.*, 2015, **98**, 2035–2044.
7 M. C. DeSantis, J. H. Kim, H. Song, P. J. Klasse and W. Cheng, *J. Biolumin. Chemilumin.*, 2016, **291**, 13088–13097.
8 J. C. Gadd, B. S. Fujimoto, S. M. Bajjalieh and D. T. Chiu, *Anal. Chem.*, 2012, **84**, 10522–10525.
9 S. W. Paddock, *BioTechniques*, 1999, **27**, 992–1004.
10 P. Hinterdorfer, M. F. Garcia-Parajo and Y. F. Dufrene, *Acc. Chem. Res.*, 2012, **45**, 327–336.
11 A. Bootz, V. Vogel, D. Schubert and J. Kreuter, *Eur. J. Pharm. Biopharm.*, 2004, **57**, 369–375.
12 C. E. Carlton and P. J. Ferreira, *Micron*, 2012, **43**, 1134–1139.
13 N. Starostina, M. Brodsky, S. Prikhodko, C. M. Hoo, M. L. Mecartney and P. West, *J. Cosmet. Sci.*, 2008, **59**, 225–232.
14 Q. K. Ong, J. Reguera, P. J. Silva, M. Moglianetti, K. Harkness, M. Longobardi, K. S. Mali, C. Renner, S. De Feyter and F. Stellacci, *ACS Nano*, 2013, **7**, 8529–8539.
15 M. Wright, in *Nanoparticles in Biology and Medicine: Methods and Protocols*, ed. M. Soloviev, Humana Press, Totowa, NJ, 2012, pp. 511–524.
16 R. W. DeBlois and C. P. Bean, *Rev. Sci. Instrum.*, 1970, **41**, 909–916.
17 J. L. Fraikin, T. Teesalu, C. M. McKenney, E. Ruoslahti and A. N. Cleland, *Nat. Nanotechnol.*, 2011, **6**, 308–313.
18 D. K. Wood, M. V. Requa and A. N. Cleland, *Rev. Sci. Instrum.*, 2007, **78**(10), 104301.
19 M. Ugawa, C. Lei, T. Nozawa, T. Ideguchi, D. Di Carlo, S. Ota, Y. Ozeki and K. Goda, *Opt. Lett.*, 2015, **40**, 4803–4806.
20 D. Holmes, H. Morgan and N. G. Green, *Biosens. Bioelectron.*, 2006, **21**, 1621–1630.
21 Y. Pang, H. Song, J. H. Kim, X. Hou and W. Cheng, *Nat. Nanotechnol.*, 2014, **9**, 624–630.
22 F. V. Ignatovich and L. Novotny, *Rev. Sci. Instrum.*, 2003, **74**, 5231–5235.
23 Y. Pang, H. Song and W. Cheng, *Biomed. Opt. Express*, 2016, **7**, 1672.
24 I. Heller, G. Sitters, O. D. Broekmans, G. Farge, C. Menges, W. Wende, S. W. Hell, E. J. G. Peterman and G. J. L. Wuite, *Nat. Methods*, 2013, **10**, 910–916.
25 C. N. Lafratta, *Anal. Bioanal. Chem.*, 2013, **405**, 5671–5677.
26 B. Redding, M. Schwab and Y. Le Pan, *Sensors*, 2015, **15**, 19021–19046.
27 F. Pierini, K. Zembrzycki, P. Nakielski, S. Pawłowska and T. A. Kowalewski, *Meas. Sci. Technol.*, 2016, **27**, 25904.
28 T. Brans, F. Strubbe, C. Schreuer, K. Neyts and F. Beunis, *J. Appl. Phys.*, 2015, **117**, 214704.
29 C.-Y. Li, D. Cao, C.-B. Qi, H.-L. Chen, Y.-T. Wan, Y. Lin, Z.-L. Zhang, D.-W. Pang and H.-W. Tang, *Biosens. Bioelectron.*, 2017, **90**, 146–152.
30 T. A. Wood, G. S. Roberts, S. Eaimkhong and P. Bartlett, *Faraday Discuss.*, 2007, **137**, 319–333.
31 A. A. P. Trichet, P. R. Dolan, D. James, G. M. Hughes, C. Vallance and J. M. Smith, *Nano Lett.*, 2016, **16**, 6172–6177.
32 N.-T. Huang, H.-L. Zhang, M.-T. Chung, J. H. Seo and K. Kurabayashi, *Lab Chip*, 2014, **14**, 1230–1245.
33 J. M. Nascimento, J. L. Nascimento, E. L. Botvinick, L. Z. Shi, B. Durrant and M. W. Berns, *J. Biomed. Opt.*, 2010, **11**, 44001.
34 A. S. Fauci, G. Pantaleo, S. Stanley and D. Weissman, *Ann. Intern. Med.*, 1996, **124**, 654–663.
35 F. Gottschalk, T. Sonderer, R. W. Scholz and B. Nowack, *Environ. Sci. Technol.*, 2009, **43**, 9216–9222.
36 K. Visscher, S. P. Gross and S. M. Block, *IEEE J. Sel. Top. Quantum Electron.*, 1996, **2**, 1066–1076.
37 D. G. Grier, *Nature*, 2003, **424**, 810–816.
38 M. Righini, A. Zelenina and R. Quidant, *2007 IEEE/LEOS Int. Conf. Opt. MEMS Nanophotonics, OMENS*, 2007, pp. 61–62.
39 M. Soltani, J. Lin, R. A. Forties, J. T. Inman, S. N. Saraf, R. M. Fulbright, M. Lipson and M. D. Wang, *Nat. Nanotechnol.*, 2014, **9**, 448–452.
40 P. Kukura, H. Ewers, C. Müller, A. Renn, A. Helenius and V. Sandoghdar, *Nat. Methods*, 2009, **6**, 923–927.
41 P. Kang, P. Schein, X. Serey, D. O'Dell and D. Erickson, *Sci. Rep.*, 2015, **5**, 12087.
42 M. Lake, M. Lake, C. Narciso, K. Cowdrick, T. Storey, S. Zhang, J. Zartman and D. Hoelzle, *Protoc. Exch.*, 2015, 1–26.
43 D. C. Duffy, J. C. McDonald, O. J. A. Schueller and G. M. Whitesides, *Anal. Chem.*, 1998, **70**, 4974–4984.
44 W. Cheng, X. Hou and F. Ye, *Opt. Lett.*, 2010, **35**, 2988–2990.
45 F. Gittes and C. F. Schmidt, *Opt. Lett.*, 1998, **23**, 7.
46 W. Cheng, S. G. Arunajadai, J. R. Moffitt, I. Tinoco and C. Bustamante, *Science*, 2011, **333**, 1746–1749.
47 S. F. Tolić-Nørrelykke, E. Schäffer, J. Howard, F. S. Pavone, F. Jülicher and H. Flyvbjerg, *Rev. Sci. Instrum.*, 2006, **77**(10), 103101.
48 A. A. Bui, A. B. Stilgoe, N. Khatibzadeh, T. A. Nieminen, M. W. Berns and H. Rubinsztein-Dunlop, *Opt. Express*, 2015, **23**, 24317–24330.
49 K. Berg-Sørensen and H. Flyvbjerg, *Rev. Sci. Instrum.*, 2004, **75**, 594–612.

